Eur. Phys. J. C 21, 399–410 (2001)
Digital Object Identifier (DOI) 10.1007/s100520100764

THE EUROPEAN PHYSICAL JOURNAL C

Measurement of $|V_{ub}|$ using b hadron semileptonic decay

The OPAL Collaboration

G. Abbiendi[2], C. Ainsley[5], P.F. Åkesson[3], G. Alexander[22], J. Allison[16], G. Anagnostou[1], K.J. Anderson[9], S. Arcelli[17], S. Asai[23], D. Axen[27], G. Azuelos[18,a], I. Bailey[26], E. Barberio[8], R.J. Barlow[16], R.J. Batley[5], T. Behnke[25], K.W. Bell[20], P.J. Bell[1], G. Bella[22], A. Bellerive[9], S. Bethke[32], O. Biebel[32], I.J. Bloodworth[1], O. Boeriu[10], P. Bock[11], J. Böhme[25], D. Bonacorsi[2], M. Boutemeur[31], S. Braibant[8], L. Brigliadori[2], R.M. Brown[20], H.J. Burckhart[8], J. Cammin[3], R.K. Carnegie[6], B. Caron[28], A.A. Carter[13], J.R. Carter[5], C.Y. Chang[17], D.G. Charlton[1,b], P.E.L. Clarke[15], E. Clay[15], I. Cohen[22], J. Couchman[15], A. Csilling[8,i], M. Cuffiani[2], S. Dado[21], G.M. Dallavalle[2], S. Dallison[16], A. De Roeck[8], E.A. De Wolf[8], P. Dervan[15], K. Desch[25], B. Dienes[30], M.S. Dixit[6,a], M. Donkers[6], J. Dubbert[31], E. Duchovni[24], G. Duckeck[31], I.P. Duerdoth[16], E. Etzion[22], F. Fabbri[2], L. Feld[10], P. Ferrari[12], F. Fiedler[8], I. Fleck[10], M. Ford[5], A. Frey[8], A. Fürtjes[8], D.I. Futyan[16], P. Gagnon[12], J.W. Gary[4], G. Gaycken[25], C. Geich-Gimbel[3], G. Giacomelli[2], P. Giacomelli[2], D. Glenzinski[9], J. Goldberg[21], K. Graham[26], E. Gross[24], J. Grunhaus[22], M. Gruwé[8], P.O. Günther[3], A. Gupta[9], C. Hajdu[29], M. Hamann[25], G.G. Hanson[12], K. Harder[25], A. Harel[21], M. Harin-Dirac[4], M. Hauschild[8], J. Hauschildt[25], C.M. Hawkes[1], R. Hawkings[8], R.J. Hemingway[6], C. Hensel[25], G. Herten[10], R.D. Heuer[25], J.C. Hill[5], K. Hoffman[9], R.J. Homer[1], D. Horváth[29,c], K.R. Hossain[28], R. Howard[27], P. Hüntemeyer[25], P. Igo-Kemenes[11], K. Ishii[23], A. Jawahery[17], H. Jeremie[18], C.R. Jones[5], P. Jovanovic[1], T.R. Junk[6], N. Kanaya[26], J. Kanzaki[23], G. Karapetian[18], D. Karlen[6], V. Kartvelishvili[16], K. Kawagoe[23], T. Kawamoto[23], R.K. Keeler[26], R.G. Kellogg[17], B.W. Kennedy[20], D.H. Kim[19], K. Klein[11], A. Klier[24], S. Kluth[32], T. Kobayashi[23], M. Kobel[3], T.P. Kokott[3], S. Komamiya[23], R.V. Kowalewski[26], T. Krämer[25], T. Kress[4], P. Krieger[6], J. von Krogh[11], D. Krop[12], T. Kuhl[3], M. Kupper[24], P. Kyberd[13], G.D. Lafferty[16], H. Landsman[21], D. Lanske[14], I. Lawson[26], J.G. Layter[4], A. Leins[31], D. Lellouch[24], J. Letts[12], L. Levinson[24], J. Lillich[10], C. Littlewood[5], S.L. Lloyd[13], F.K. Loebinger[16], G.D. Long[26], M.J. Losty[6,a], J. Lu[27], J. Ludwig[10], A. Macchiolo[18], A. Macpherson[28,l], W. Mader[3], S. Marcellini[2], T.E. Marchant[16], A.J. Martin[13], J.P. Martin[18], G. Martinez[17], G. Masetti[2], T. Mashimo[23], P. Mättig[24], W.J. McDonald[28], J. McKenna[27], T.J. McMahon[1], R.A. McPherson[26], F. Meijers[8], P. Mendez-Lorenzo[31], W. Menges[25], F.S. Merritt[9], H. Mes[6,a], A. Michelini[2], S. Mihara[23], G. Mikenberg[24], D.J. Miller[15], S. Moed[21], W. Mohr[10], T. Mori[23], A. Mutter[10], K. Nagai[13], I. Nakamura[23], H.A. Neal[33], R. Nisius[8], S.W. O'Neale[1], A. Oh[8], A. Okpara[11], M.J. Oreglia[9], S. Orito[23], C. Pahl[32], G. Pásztor[8,i], J.R. Pater[16], G.N. Patrick[20], J.E. Pilcher[9], J. Pinfold[28], D.E. Plane[8], B. Poli[2], J. Polok[8], O. Pooth[8], A. Quadt[3], K. Rabbertz[8], C. Rembser[8], P. Renkel[24], H. Rick[4], N. Rodning[28], J.M. Roney[26], S. Rosati[3], K. Roscoe[16], Y. Rozen[21], K. Runge[10], D.R. Rust[12], K. Sachs[6], T. Saeki[23], O. Sahr[31], E.K.G. Sarkisyan[8,m], C. Sbarra[26], A.D. Schaile[31], O. Schaile[31], P. Scharff-Hansen[8], M. Schröder[8], M. Schumacher[25], C. Schwick[8], W.G. Scott[20], R. Seuster[14,g], T.G. Shears[8,j], B.C. Shen[4], C.H. Shepherd-Themistocleous[5], P. Sherwood[15], A. Skuja[17], A.M. Smith[8], G.A. Snow[17], R. Sobie[26], S. Söldner-Rembold[10,e], S. Spagnolo[20], F. Spano[9], M. Sproston[20], A. Stahl[3], K. Stephens[16], D. Strom[19], R. Ströhmer[31], L. Stumpf[26], B. Surrow[25], S. Tarem[21], M. Tasevsky[8], R.J. Taylor[15], R. Teuscher[9], J. Thomas[15], M.A. Thomson[5], E. Torrence[19], D. Toya[23], T. Trefzger[31], A. Tricoli[2], I. Trigger[8], Z. Trócsányi[30,f], E. Tsur[22], M.F. Turner-Watson[1], I. Ueda[23], B. Ujvári[30,f], B. Vachon[26], C.F. Vollmer[31], P. Vannerem[10], M. Verzocchi[17], H. Voss[8], J. Vossebeld[8], D. Waller[6], C.P. Ward[5], D.R. Ward[5], P.M. Watkins[1], A.T. Watson[1], N.K. Watson[1], P.S. Wells[8], T. Wengler[8], N. Wermes[3], D. Wetterling[11] G.W. Wilson[16], J.A. Wilson[1], T.R. Wyatt[16], S. Yamashita[23], V. Zacek[18], D. Zer-Zion[8,k]

[1] School of Physics and Astronomy, University of Birmingham, Birmingham B15 2TT, UK
[2] Dipartimento di Fisica dell' Università di Bologna and INFN, 40126 Bologna, Italy
[3] Physikalisches Institut, Universität Bonn, 53115 Bonn, Germany
[4] Department of Physics, University of California, Riverside CA 92521, USA
[5] Cavendish Laboratory, Cambridge CB3 0HE, UK
[6] Ottawa-Carleton Institute for Physics, Department of Physics, Carleton University, Ottawa, Ontario K1S 5B6, Canada
[8] CERN, European Organisation for Nuclear Research, 1211 Geneva 23, Switzerland
[9] Enrico Fermi Institute and Department of Physics, University of Chicago, Chicago IL 60637, USA
[10] Fakultät für Physik, Albert Ludwigs Universität, 79104 Freiburg, Germany
[11] Physikalisches Institut, Universität Heidelberg, 69120 Heidelberg, Germany
[12] Indiana University, Department of Physics, Swain Hall West 117, Bloomington IN 47405, USA
[13] Queen Mary and Westfield College, University of London, London E1 4NS, UK

[14] Technische Hochschule Aachen, III Physikalisches Institut, Sommerfeldstrasse 26-28, 52056 Aachen, Germany
[15] University College London, London WC1E 6BT, UK
[16] Department of Physics, Schuster Laboratory, The University, Manchester M13 9PL, UK
[17] Department of Physics, University of Maryland, College Park, MD 20742, USA
[18] Laboratoire de Physique Nucléaire, Université de Montréal, Montréal, Quebec H3C 3J7, Canada
[19] University of Oregon, Department of Physics, Eugene OR 97403, USA
[20] CLRC Rutherford Appleton Laboratory, Chilton, Didcot, Oxfordshire OX11 0QX, UK
[21] Department of Physics, Technion-Israel Institute of Technology, Haifa 32000, Israel
[22] Department of Physics and Astronomy, Tel Aviv University, Tel Aviv 69978, Israel
[23] International Centre for Elementary Particle Physics and Department of Physics, University of Tokyo, Tokyo 113-0033, and Kobe University, Kobe 657-8501, Japan
[24] Particle Physics Department, Weizmann Institute of Science, Rehovot 76100, Israel
[25] Universität Hamburg/DESY, II Institut für Experimental Physik, Notkestrasse 85, 22607 Hamburg, Germany
[26] University of Victoria, Department of Physics, P O Box 3055, Victoria BC V8W 3P6, Canada
[27] University of British Columbia, Department of Physics, Vancouver BC V6T 1Z1, Canada
[28] University of Alberta, Department of Physics, Edmonton AB T6G 2J1, Canada
[29] Research Institute for Particle and Nuclear Physics, 1525 Budapest, P O Box 49, Hungary
[30] Institute of Nuclear Research, 4001 Debrecen, P O Box 51, Hungary
[31] Ludwigs-Maximilians-Universität München, Sektion Physik, Am Coulombwall 1, 85748 Garching, Germany
[32] Max-Planck-Institute für Physik, Föhring Ring 6, 80805 München, Germany
[33] Yale University, Department of Physics, New Haven, CT 06520, USA

Received: 26 June 2001 /
Published online: 31 August 2001 –

Abstract. The magnitude of the CKM matrix element $|V_{ub}|$ is determined by measuring the inclusive charmless semileptonic branching fraction of beauty hadrons at OPAL based on $b \to X_u \ell\nu$ event topology and kinematics. This analysis uses OPAL data collected between 1991 and 1995, which correspond to about four million hadronic Z decays. We measure $\mathrm{Br}(b \to X_u \ell\nu)$ to be $(1.63 \pm 0.53\ ^{+0.55}_{-0.62}) \times 10^{-3}$. The first uncertainty is the statistical error and the second is the systematic error. From this analysis, $|V_{ub}|$ is determined to be:

$$|V_{ub}| = (4.00 \pm 0.65(\mathrm{stat})^{+0.67}_{-0.76}(\mathrm{sys}) \pm 0.19(\mathrm{HQE})) \times 10^{-3}.$$

The last error represents the theoretical uncertainties related to the extraction of $|V_{ub}|$ from $\mathrm{Br}(b \to X_u \ell\nu)$ using the Heavy Quark Expansion.

1 Introduction

The CKM matrix [1] describes the relation between quark weak and mass eigenstates, with the element V_{ub} describing decays of the b to u quark. Its magnitude, $|V_{ub}|$, can be calculated by measuring the inclusive $b \to u$ semileptonic decay rate. Given that the branching fraction of inclusive $b \to u$ semileptonic decay is of order 10^{-3}, a large number of b hadrons are required to measure $|V_{ub}|$. The dominant background to $b \to X_u \ell\nu$ comes from $b \to X_c \ell\nu$ decays because the branching ratio of $b \to X_c \ell\nu$ is more than 50 times greater than that of $b \to X_u \ell\nu$. Here the lepton ℓ refers to either an electron or a muon, and b denotes all weakly decaying b hadrons[1]. X_u and X_c represent hadronic states resulting from a b quark semileptonic decay to a u or c quark respectively. The determination of $|V_{ub}|$ depends on the b to u and b to c semileptonic decay models.

The inclusive method developed by ARGUS [2] and CLEO [3] is to extract $|V_{ub}|/|V_{cb}|$ from the excess of events in the 2.3 to 2.6 GeV/c region of the lepton momentum spectrum in the B meson rest frame, where the $b \to X_c \ell\nu$ contributions vanish. This technique uses only a small fraction of the lepton phase space and so has considerable model dependence in extrapolating to the entire lepton spectrum in the B rest frame. In addition, since the LEP experiments can not precisely determine the B meson rest frame, this method is not appropriate for the LEP experiments. Instead, at LEP, $|V_{ub}|$ or $|V_{ub}|/|V_{cb}|$ is extracted using a larger portion of the lepton spectrum as well as other kinematic variables. The inclusive measurement of the branching fraction of the $b \to X_u \ell\nu$ decay

[a] and at TRIUMF, Vancouver, Canada V6T 2A3
[b] and Royal Society University Research Fellow
[c] and Institute of Nuclear Research, Debrecen, Hungary
[e] and Heisenberg Fellow
[f] and Department of Experimental Physics, Lajos Kossuth University, Debrecen, Hungary
[g] and MPI München
[i] and Research Institute for Particle and Nuclear Physics, Budapest, Hungary
[j] now at University of Liverpool, Dept of Physics, Liverpool L69 3BX, UK
[k] and University of California, Riverside, High Energy Physics Group, CA 92521, USA
[l] and CERN, EP Div, 1211 Geneva 23
[m] and Tel Aviv University, School of Physics and Astronomy, Tel Aviv 69978, Israel.

[1] Charged conjugate states are implied if not stated otherwise

has been performed at LEP by ALEPH [4], DELPHI [5] and L3 [6].

The theoretical uncertainty for the value of $|V_{ub}|$ extracted from a measurement of inclusive $b \to X_u \ell\nu$ branching fraction differs from that extracted from measurements of exclusive b $\to$ u semileptonic decay rates. A recent theoretical study concludes that there is a 5% theoretical uncertainty on $|V_{ub}|$ values derived from $b \to X_u \ell\nu$ inclusive measurements [7], using the Heavy Quark Expansion. There is a 15% theoretical uncertainty associated with $|V_{ub}|$ values extracted from measurements of the exclusive branching fractions B $\to \pi\ell\nu$ or B $\to \rho\ell\nu$ [8], interpreted within the framework of the Heavy Quark Effective Theory (HQET).

In this paper, we describe the determination of $|V_{ub}|$ using the inclusive $b \to X_u \ell\nu$ decay rate from the OPAL data taken at center of mass energies near the Z resonance. The event preselection, the $b \to X_u \ell\nu$ decay models and the neural network used to separate $b \to X_u \ell\nu$ from the background will be discussed in detail in the following sections.

2 The OPAL detector, data and Monte Carlo samples

The OPAL detector is a multi-purpose 4π spectrometer incorporating excellent charged and neutral particle detection capabilities. The OPAL detector is described in detail elsewhere [9]. A brief description is given here. The central tracking system consists of a silicon microvertex detector, a vertex chamber, a jet chamber and z chambers. The momentum of tracks and the primary and secondary vertex position are reconstructed by the central tracking system, which is located inside a solenoid. The solenoid provides a magnetic field of 0.435T. Outside the solenoid is the electromagnetic calorimeter, which is composed of lead glass blocks and is used to measure the energies and positions of electrons and photons. The hadron calorimeter lies outside the electromagnetic calorimeter and is used to measure the energy of hadrons emerging from the electromagnetic calorimeter and assists in the identification of muons. The outermost OPAL detector is the muon detector which consists of a system of barrel and endcap muon chambers. A large fraction of muons with momenta less than 2 GeV/c are absorbed by the other detectors or the iron shielding before reaching the muon chambers.

The current analysis uses OPAL 1991 to 1995 data, collected near the Z resonance, comprising about four million hadronic Z decays. Monte Carlo simulated events were generated using the JETSET 7.4 [10] generator, with parameters described in [11]. Approximately five million hadronic Z $\to$ b$\bar{\text{b}}$ decays were generated to study the $b \to X_c \ell\nu$ decay and the b $\to$ c $\to \ell$ cascade decay. Six million hadronic Z $\to$ q$\bar{\text{q}}$ (where q can be u, d, s, c and b) decays were generated to study the leptons from primary charm quarks and light quarks. Two hundred thousand events from a $b \to X_u \ell\nu$ hybrid model [12] were produced to simulate the b $\to$ u semileptonic decay. The hybrid model will be described in detail in Sect. 3.1.

3 Signal and background simulation

The b to u semileptonic decay and background simulation are described below. The b to u semileptonic decay and background simulated events are passed through the full OPAL detector simulation [13] to produce the corresponding response. For this paper, the production fractions of B^+, B^0, B_s^0 and Λ_b in Z decays were adjusted to reproduce those given by the Particle Data Group [14].

3.1 The $b \to X_u \ell\nu$ hybrid model

Several theoretical models have been proposed for the $b \to X_u \ell\nu$ decay. Exclusive bound-state models [15–18] approximate the inclusive $b \to X_u \ell\nu$ lepton spectra by summing contributions from all the exclusive final states. These exclusive models do not include all the possible final states nor any non-resonant states and therefore yield an incomplete prediction of the inclusive lepton momentum distribution, especially in the region of high hadronic invariant mass. The inclusive free quark models [19–23] treat the heavy quark as a free quark and the final state as a quark plus gluons. Free quark models are known to give poor agreement with experiments at low u quark recoil momentum. Therefore, a hybrid model [12] has been proposed to model the $b \to X_u \ell\nu$ decay by using the exclusive model in the lower hadronic invariant mass region and using the inclusive model in the higher hadronic invariant mass region. The ISGW2 model [18] is used as the exclusive part of the hybrid model. The ACCMM model [19], combined with the W decay model [24] plus JETSET fragmentation, is used as the inclusive part of the hybrid model. Since the ISGW2 exclusive model includes the exclusive resonant final states 1S, 2S and 1P up to 1.5 GeV/c^2 in the hadronic mass, the boundary between the inclusive and exclusive parts of the hybrid model is placed at the hadronic invariant mass of 1.5 GeV/c^2. The relative normalization of the inclusive and exclusive parts of the hybrid model is determined by the inclusive model. This hybrid model is only applied to decays of B mesons. There are no theoretical predictions for b to u semileptonic transitions of b baryons. The exclusive transitions of the b baryons in the OPAL tune of JETSET [10,11] are used.

In order to estimate systematic uncertainties due to modeling of the inclusive spectrum, alternative models are also studied. Signal events were generated with the QCD universal function [20–22] and parton [23] models. The invariant mass distributions of the hadronic recoil u$\bar{\text{q}}$ system are shown in Fig. 1a for the QCD universal function, ACCMM and parton models. The invariant mass distribution of the hadronic recoil u$\bar{\text{q}}$ system for the hybrid model is shown in Fig. 1b.

3.2 Background simulation

The ACCMM model [19] is used to describe the lepton spectrum of $b \to X_c \ell\nu$ and b $\to$ c $\to \ell$ decays. The frag-

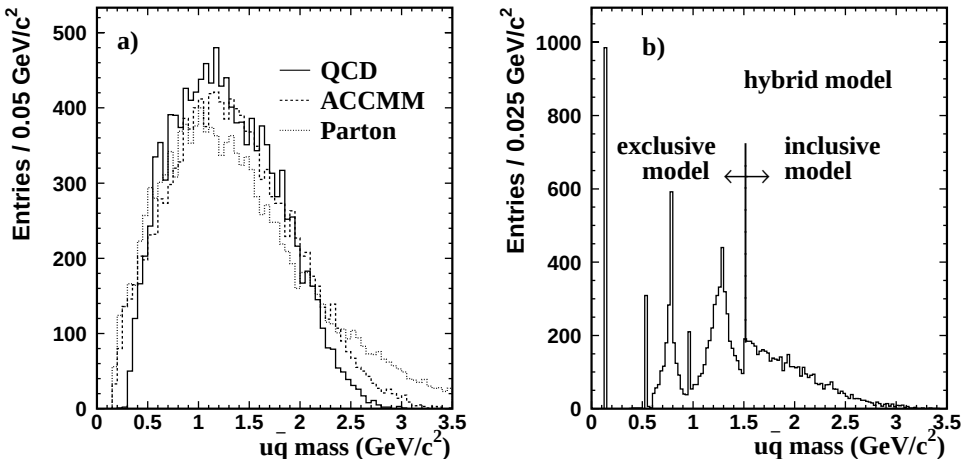

Fig. 1a,b. The $u\bar{q}$ invariant mass distributions, **a** using the QCD universal function, ACCMM and parton inclusive models, **b** using the hybrid model. Only the portion of the $u\bar{q}$ invariant mass above 1.5 GeV/c^2 from the inclusive model in **a** is used in the hybrid model. The boundary between the exclusive model (left arrow) and the inclusive model (right arrow) in the hybrid model is indicated by the dashed line in **b**

mentation function of Peterson et al. [25] is used to describe the b quark and c quark fragmentation. The branching fractions of $B^0 \to D^- \ell^+ \nu$, $B^0 \to D^{*-} \ell^+ \nu$, $B^+ \to \bar{D}^0 \ell^+ \nu$, $B^+ \to \bar{D}^{*0} \ell^+ \nu$ and $\Lambda_b \to \Lambda_c X \ell \nu$ were modified to reproduce those given by the Particle Data Group [14]. The Λ_b lepton momentum spectrum corresponding to -56% polarization [26] was used.

4 Event preselection

A hadronic event selection [27] and detector performance requirements are applied to the data. The thrust polar angle[2] $|\cos\theta|$ is required to be less than 0.9 to ensure that the events are well contained within the acceptance of the detector. The selected events must pass the b identification, the lepton selection and the b semileptonic decay selection. All these selections are described in detail in the following sections. After all these preselections, the $b \to X_u \ell \nu$ decay purity is 1.3% and the main background is from $b \to X_c \ell \nu$ decays.

4.1 b identification

A neural network algorithm [28] based on charged particle vertex information is used to separate the b flavour events from the other flavour events in each hemisphere. If either hemisphere passes this neural network selection, the event is selected. After this neural network selection, the b purity is more than 91% and the b identification selection efficiency is approximately 30% per hemisphere from the Monte Carlo simulation in which a branching fraction of 1.0×10^{-3} for the $b \to X_u \ell \nu$ transition is incorporated. Both hemispheres are searched for electron and muon candidates after the b identification.

[2] A right handed coordinate system is used, with positive z along the e^- beam direction and x pointing toward the center of the LEP ring. The polar and azimuthal angles are denoted by θ and ϕ, and the origin is taken to be the center of the detector

4.2 Lepton selection

Electrons are identified by a neural network [28] using the track and calorimeter information. The electron momentum is required to be greater than 2 GeV/c. Electrons from photon conversions, $\gamma \to e^+e^-$, contribute a significant background to the prompt electron samples. Another neural network is used to reject this background [28]. The photon conversion background is reduced by 94% after the photon conversion neural network selection, whilst retaining 98% of the selected prompt electrons. After all these requirements, the resulting electron efficiency is approximately 74% with a purity of 94% within the geometrical acceptance.

Muons are identified using reconstructed track segments in the muon chambers [28]. The muon momentum is required to be greater than 3 GeV/c. The reconstructed tracks in the central detector are extrapolated to the muon chambers to see if they match the track segments reconstructed in the external muon chambers. The measured energy loss dE/dx is also required to be consistent with the expected value for a muon. After all these requirements, the muon selection efficiency is approximately 90% and the muon purity approximately 93% within the geometrical acceptance.

Electron and muon momenta transverse to the direction of the jet containing the lepton are required to be greater than 0.5 GeV/c in order to reject leptons from light quark decay. The lepton is included in the calculation of the jet direction. The jet finding is based on the cone algorithm [29].

4.3 b semileptonic decay selection

A neural network [30] based on lepton information is used to separate the b hadron semileptonic decays, $b \to X_c \ell \nu$ and $b \to X_u \ell \nu$, from non b semileptonic decays. The distributions of the neural network output variable are shown in Fig. 2. After this neural network b semileptonic decay selection, the b hadron semileptonic decay purity is 97% and the efficiency is 65% for this neural network; the c $\to \ell$ events, where c is a primary quark, and b $\to$ c $\to \ell$ events are suppressed.

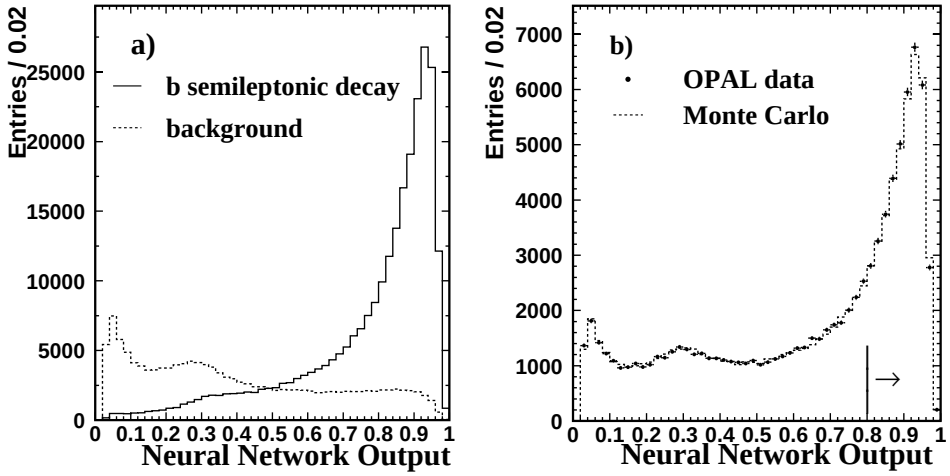

Fig. 2a,b. The b hadron semileptonic decay neural network output distributions. **a** for the b semileptonic decays and the scaled background from the Monte Carlo simulated events, here the background indicates all events excluding $b \to X_c \ell\nu$ and $b \to X_u \ell\nu$, **b** comparison between the OPAL data and the Monte Carlo simulated events. The selected region is shown by the arrow in **b**

5 $b \to X_u \ell\nu$ neural network

Because of the dominant $b \to X_c \ell\nu$ background, it is difficult to enrich the sample in $b \to X_u \ell\nu$ decays using only one kinematic variable. A multi-layered feed-forward artificial neural network based on the JETNET 3.0 program [31] is used to enrich the sample in $b \to X_u \ell\nu$ decays. There are four layers in this neural network. The neural network structure is 7-10-10-1. In the first layer, seven variables are used as inputs to the neural network. The last layer is the neural network output variable. A figure of merit [32] is used to determine the discrimination power of these seven variables in separating two classes of events, i.e. signal and background. The higher the figure of merit, the better the separation between the two classes. Over twenty kinematic variables were initially considered as inputs to the $b \to X_u \ell\nu$ neural network. Only seven variables are selected as inputs to the $b \to X_u \ell\nu$ neural network based on good separation between $b \to X_u \ell\nu$ and background and good agreement between data and Monte Carlo simulated events. These seven input variables, in order of decreasing figure of merit, are:

1. the invariant mass of the most energetic final state particle combined with the lepton,
2. the lepton energy in the b hadron rest frame, where the b hadron energy and momentum are estimated using the techniques described in [33],
3. the lepton momentum transverse to the jet axis (the jet axis calculation includes the lepton),
4. the transverse momentum of the most energetic final state hadron with respect to the lepton direction (assuming all hadrons are pions),
5. the rapidity of the most energetic final state hadron calculated with respect to the lepton direction (assuming all hadrons are pions),
6. the fraction of the reconstructed b hadron energy carried by the lepton,
7. the reconstructed hadronic invariant mass, M_x, which is calculated by:

$$M_x{}^2 = \sum_i (W_i E_i)^2 - \sum_i (W_i \vec{p}_i)^2, \qquad (1)$$

where i denotes all hadronic tracks and clusters. W_i is the probability that the i^{th} hadronic track or unassociated cluster comes from b decay and is calculated using the techniques described in [34]. E_i and $\vec{p}_i$ are the energy and momentum of the i^{th} hadronic track or neutral cluster.

Only the tracks and clusters from the same jet as the lepton are included in the calculation of these seven input variables. The seven input variable distributions for the $b \to X_u \ell\nu$ and the background in the Monte Carlo simulation are shown in Fig. 3. The agreement between the Monte Carlo simulated events and the OPAL data for these seven variables is shown in Fig. 4.

Twelve thousand $b \to X_u \ell\nu$ events, which were simulated with the hybrid model and have passed the event preselection, and the same number of background events from the multi-hadron $Z \to q\bar{q}$ Monte Carlo simulation after the preselection are used to train the $b \to X_u \ell\nu$ neural network. Two other samples of signal and background events of the same size are used to test the neural network performance. The neural network output distributions from $b \to X_u \ell\nu$ and background are shown in Fig. 5a.

The background composition from the $b \to X_u \ell\nu$ neural network is shown in Fig. 5b. Ninety percent of the background in this analysis comes from the $b \to X_c \ell\nu$ decay, 6.8% from the b → c decay with the c subsequently decaying to a lepton. Another 0.6% comes from the $c \to \ell$ decay in which the c quark is the primary quark. Other background processes make up the remaining 2.6%, of which 36% is from the $b \to \tau$ decay with the τ subsequently decaying to an electron or a muon, and most of the rest of the background is from a pion or a kaon misidentified as an electron or a muon.

6 Extraction of Br($b \to X_u \ell\nu$)

The branching fraction of $b \to X_u \ell\nu$ decay can be obtained from the best fit of the Monte Carlo simulated events to OPAL data based on the $b \to X_u \ell\nu$ neural network output

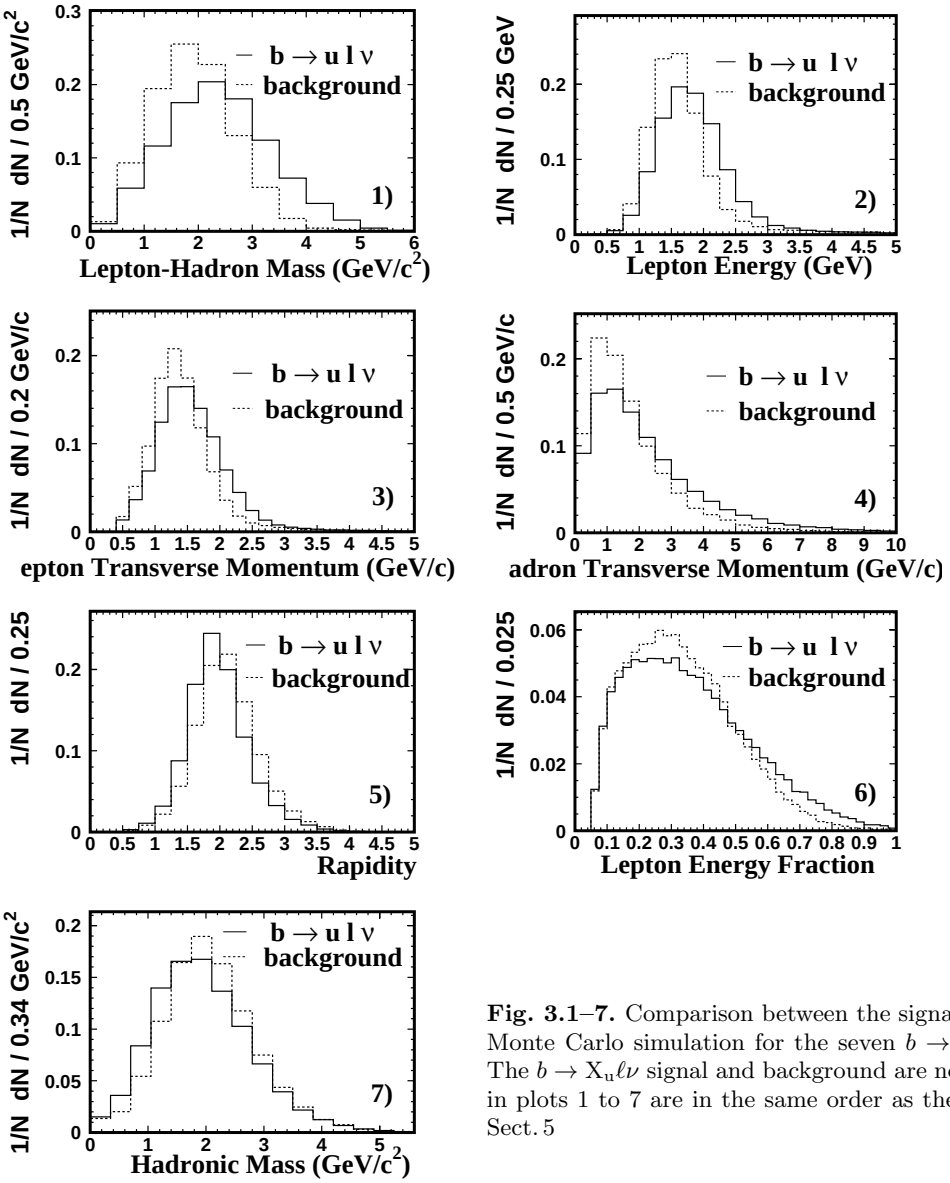

Fig. 3.1–7. Comparison between the signal $b \to X_u \ell\nu$ and the background in the Monte Carlo simulation for the seven $b \to X_u \ell\nu$ neural network input variables. The $b \to X_u \ell\nu$ signal and background are normalized to unity. The input variables in plots 1 to 7 are in the same order as the input variables defined in the text of Sect. 5

distributions. $\mathrm{Br}(b \to X_u \ell\nu)$ is extracted from the $b \to X_u \ell\nu$ neural network output distributions by minimizing:

$$\chi^2 = \sum_k \frac{[N_k^{\mathrm{data}} - N_{\mathrm{data}}(x\ f_k^{\mathrm{MC_{bu}}} + (1-x) f_k^{\mathrm{MC_{bg}}})]^2}{N_k^{\mathrm{data}}}, \quad (2)$$

where N_k^{data} is the number of events from the data in the k^{th} bin of the neural network output. N_{data} is the total number of events in the data after preselection. The free parameter x is the fraction of signal events in the data after preselection, which can be converted to $\mathrm{Br}(b \to X_u \ell\nu)$ based on the number of signal events and the number of background events in the Monte Carlo simulation after preselection. $f_k^{\mathrm{MC_{bu}}}$ is the fraction of simulated signal events in the k^{th} bin of the $b \to X_u \ell\nu$ neural network output with respect to the total number of simulated signal events after preselection. $f_k^{\mathrm{MC_{bg}}}$ is the fraction of simulated background events in the k^{th} bin of the $b \to X_u \ell\nu$ neural network output with respect to the total number of simulated background events after preselection. Here the background includes $b \to X_c \ell\nu$, $b \to c \to \ell$, $c \to \ell$ and other contributions. The sum over the index k is performed from the neural network cut to the last bin in the neural network output distribution. The $\mathrm{Br}(b \to X_u \ell\nu)$ from the fit result x, as well as its statistical and systematic errors, depends on the $b \to X_u \ell\nu$ neural network cut. The resulting $\mathrm{Br}(b \to X_u \ell\nu)$ is stable, with variations less than 0.2×10^{-3}, as the neural network cut varies in value from 0.3 to 0.8. A neural network cut of 0.7 is chosen to minimize the total relative errors and yields

$$\mathrm{Br}(b \to X_u \ell\nu) = (1.63 \pm 0.53) \times 10^{-3},$$

where the uncertainty is the statistical error only.

In Fig. 6a, the neural network output distribution from data and the Monte Carlo simulation events with no $b \to X_u \ell\nu$ semileptonic decay is shown and the excess of events in the data can be seen in the last bin. Here the distribution of Monte Carlo simulated events with no $b \to X_u \ell\nu$

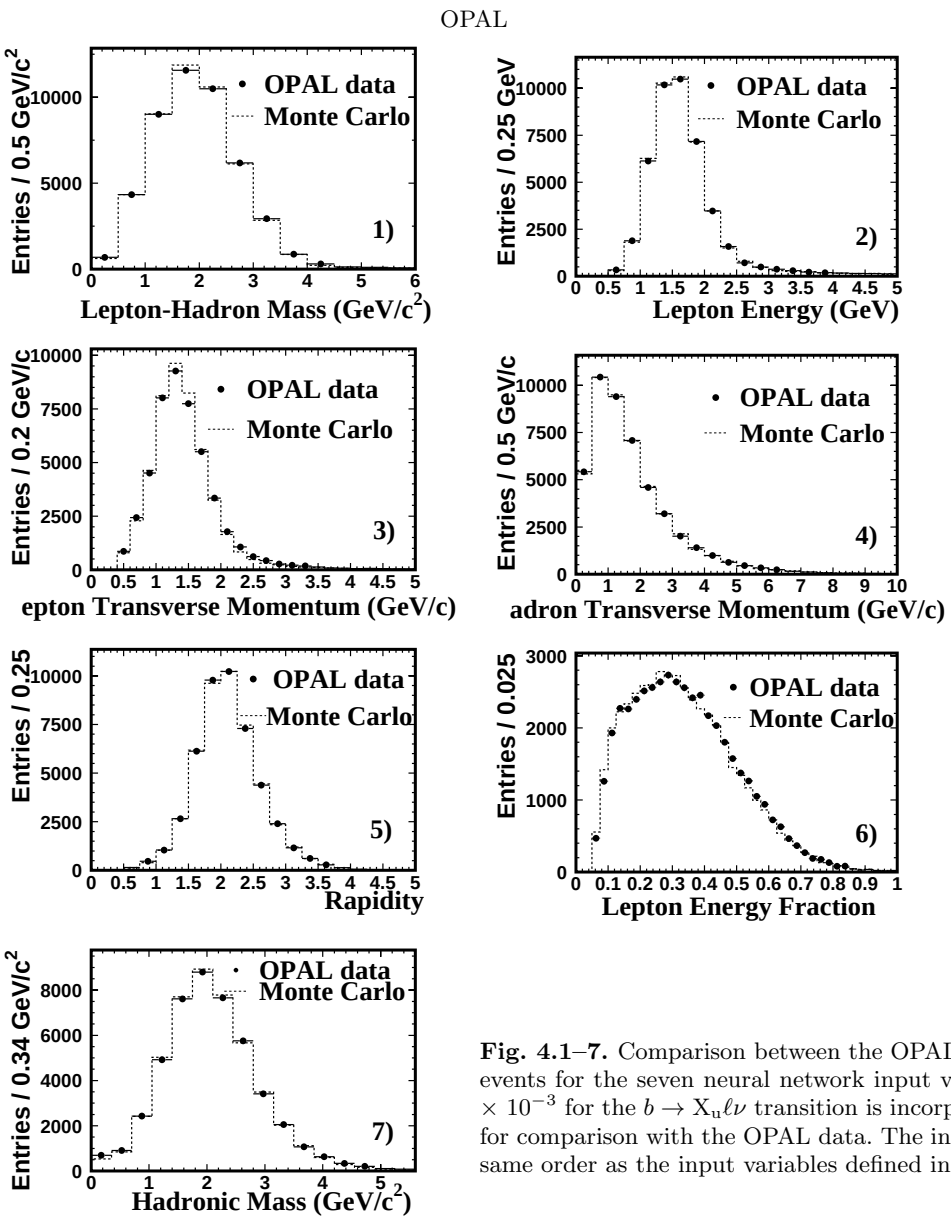

Fig. 4.1–7. Comparison between the OPAL data and the Monte Carlo simulated events for the seven neural network input variables. A branching fraction of 1.63 $\times 10^{-3}$ for the $b \to X_u \ell\nu$ transition is incorporated in the Monte Carlo simulation for comparison with the OPAL data. The input variables in plots 1 to 7 are in the same order as the input variables defined in the text of Sect. 5

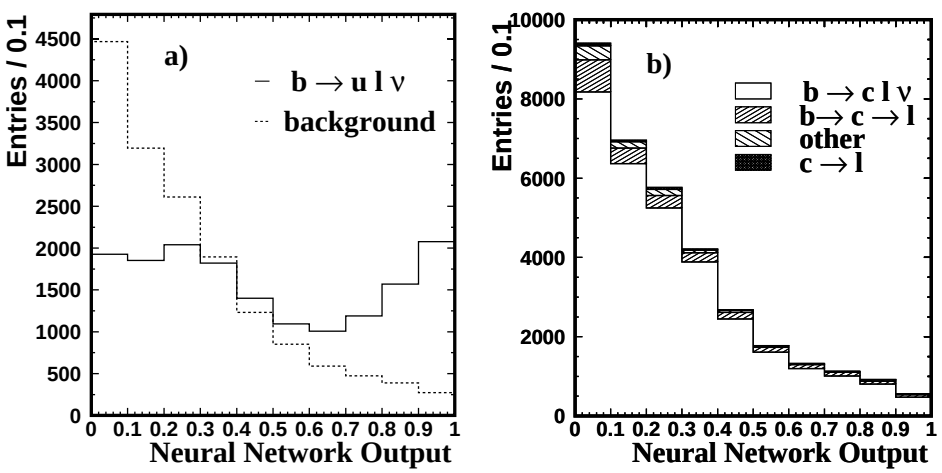

Fig. 5a,b. The $b \to X_u \ell\nu$ neural network output distributions, **a** for $b \to X_u \ell\nu$ and background, **b** for different background components

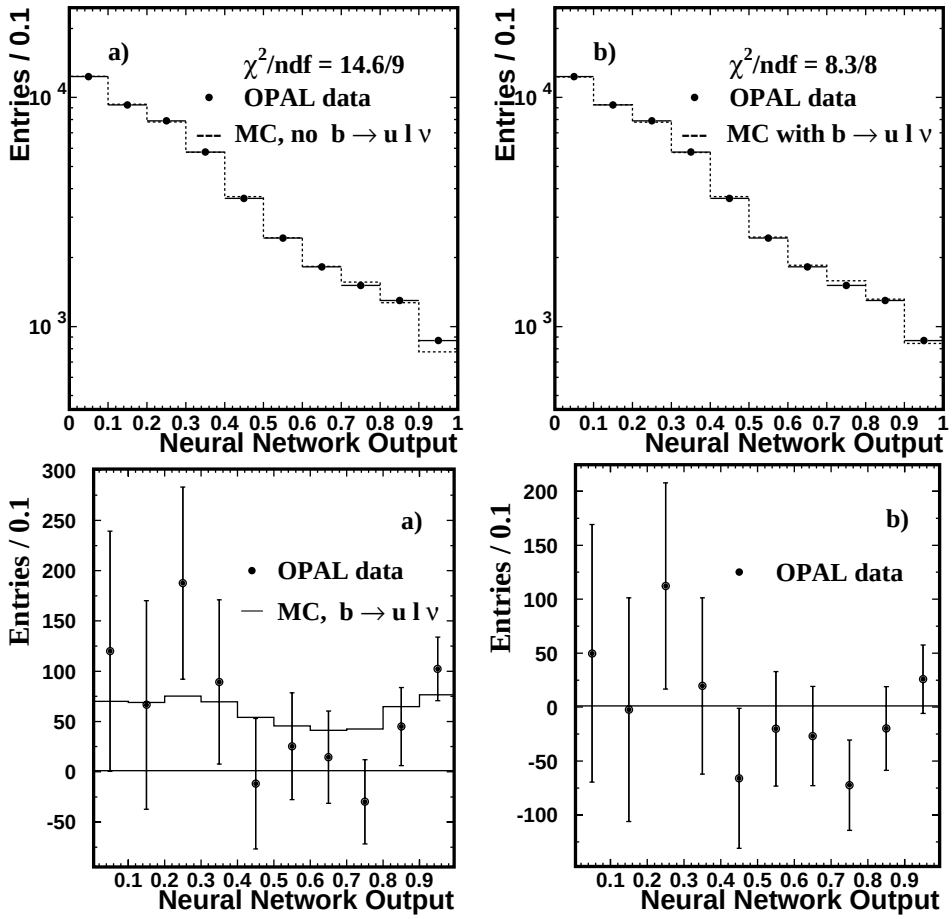

Fig. 6a,b. The neural network output distributions for data and Monte Carlo simulated events, **a** with no $b \to X_u \ell\nu$ transition in the Monte Carlo simulated events, **b** with a branching fraction of 1.63 $\times$ 10^{-3} $b \to X_u \ell\nu$ decay incorporated. The distribution of Monte Carlo simulated events is normalized to the data for both plots

Fig. 7a,b. The neural network output distributions. **a** Data after subtracting the background from the Monte Carlo simulated events (points) show agreement with the simulated $b \to X_u \ell\nu$ signal (solid histogram). **b** Data after subtracting the Monte Carlo simulated events with a branching fraction of 1.63×10^{-3} $b \to X_u \ell\nu$ decay incorporated. Here the error bars include the statistical error from data and Monte Carlo simulated events

transitions is normalized to the same number of entries as the data. The χ^2/ndf is 14.6/9, which corresponds to a 10% confidence level, assuming no contributions from $b \to X_u \ell\nu$ transition. Here the χ^2 is calculated by summing over all bins in the neural network output distribution. When the $b \to X_u \ell\nu$ transition is incorporated in the Monte Carlo simulation with a branching fraction of 1.63 $\times$ 10^{-3}, the Monte Carlo simulation agrees much better with the data, as can be seen in Fig. 6b. The χ^2/ndf is then 8.3/8, corresponding to a 41% confidence level.

The data after subtracting the background from the Monte Carlo simulated events agree well with the simulated $b \to X_u \ell\nu$ signal within statistical errors, which is shown in Fig. 7.

A series of cross checks, dividing the lepton samples into electron and muon samples and dividing the data into two samples for the years 1991 to 1993 and the years 1994 to 1995, are performed. The Br($b \to X_u \ell\nu$) results are consistent within statistical errors for these cross checks.

7 Systematic errors

The list of systematic errors is given in Table 1. Unless otherwise specified, the systematic errors are estimated by varying each parameter described by one standard deviation and taking the corresponding largest errors. The resulting systematic errors in Table 1 are discussed in detail:

b quark fragmentation: Many parameterizations have been suggested to describe the heavy quark fragmentation process. The Peterson function [25] is used here to simulate the b and c fragmentation in the Monte Carlo simulation. The systematic error in the b quark fragmentation is estimated by varying the b hadron mean scaled energy $\langle x_E \rangle_b$ within the experimental range 0.702 ± 0.008 recommended by the LEP Electroweak Working Group [35]. This value is consistent with a recent determination of $\langle x_E \rangle_b = 0.714 \pm 0.009$ from SLD [37]. The systematic error is also estimated from the Collins and Spiller fragmentation function [38] and Kartvelishvili fragmentation function [39]. The uncertainties in c quark fragmentation can be neglected because the background from $c \to \ell$, where c is a primary quark, is very small.

$b \to X_c \ell\nu$ lepton momentum spectrum modeling: Different decay models are used to predict the lepton spectrum in the b hadron rest frame for the $b \to X_c \ell\nu$ decay. Although all models are derived for B^0 and B^+ semileptonic decay only, they are extrapolated to the B_s and Λ_b semileptonic decay. This will be correct in the simple spectator model and is a reasonable approximation for this analysis. The lepton spectrum from the ACCMM model [19] is used as a base model for the $b \to X_c \ell\nu$ decay. The systematic errors due to $b \to X_c \ell\nu$ lepton momentum spectrum modeling are estimated from the ISGW [16] and ISGW** [36]

Table 1. Systematic errors for $\mathrm{Br}(b \to X_u \ell\nu)$

Error Source	Variation or value and variation	$\Delta\mathrm{Br}(b \to \mathrm{X_u}\ell\nu)$ 10^{-3}
Fragmentation $\langle x_\mathrm{E}\rangle_\mathrm{b}$	0.702 ± 0.008 [35]	$^{+0.28}_{-0.32}$
Lepton spectrum (b $\to$ c)	ISGW** [36], ISGW [16]	$^{+0.18}_{-0.29}$
MC statistics	(see text)	± 0.22
b and c hadron semileptonic decay	(see text)	± 0.19
MC modeling	(see text)	± 0.19
$b \to \mathrm{X_u}\ell\nu$ modeling error (hybrid)	(see text)	± 0.19
$b \to \mathrm{X_u}\ell\nu$ modeling error (inclusive)	Parton [23], QCD [20]	± 0.14
$b \to \mathrm{X_u}\ell\nu$ modeling error (exclusive)	ISGW2 [18], JETSET	± 0.07
Tracking resolution	$\pm 10\%$ [28]	± 0.07
c hadron decay multiplicity	(see text)	± 0.07
Λ_b production rate	$(11.6 \pm 2.0)\%$ [14]	∓ 0.04
Λ_b polarization	$-0.56\ ^{+0.22}_{-0.16}$	± 0.03
Electron ID efficiency	$\pm 4\%$ [28]	∓ 0.04
Muon ID efficiency	$\pm 2\%$ [30]	∓ 0.03
Electron fake rate	$\pm 21\%$ [28]	∓ 0.02
Muon fake rate	$\pm 8\%$ [28]	∓ 0.01
$\mathrm{Br}(b \to \mathrm{X}\tau\bar{\nu}_\tau)$	$(2.6 \pm 0.4)\%$ [14]	± 0.01
b lifetime	(1.564 ± 0.014) ps [14]	< 0.01
$\mathrm{R_b}$	0.21644 ± 0.00075 [14]	< 0.01
Total		$^{+0.55}_{-0.62}$

Table 2. Systematic errors for $\mathrm{Br}(b \to \mathrm{X_u}\ell\nu)$ from uncertainties of the b hadron and c hadron semileptonic decay branching ratios

Error Source	Variation	$\Delta\mathrm{Br}(b \to \mathrm{X_u}\ell\nu)(10^{-3})$
$\mathrm{Br}(\mathrm{B^0} \to \mathrm{D^-}\ell^+\nu)$	$(2.10 \pm 0.19)\%$ [14]	∓ 0.02
$\mathrm{Br}(\mathrm{B^0} \to \mathrm{D^{*-}}\ell^+\nu)$	$(4.60 \pm 0.27)\%$ [14]	± 0.03
$\mathrm{Br}(\mathrm{B^+} \to \bar{\mathrm{D}}^0\ell^+\nu)$	$(2.15 \pm 0.22)\%$ [14]	∓ 0.06
$\mathrm{Br}(\mathrm{B^+} \to \bar{\mathrm{D}}^{*0}\ell^+\nu)$	$(5.3 \pm 0.8)\%$ [14]	± 0.04
$\mathrm{Br}(\bar{\mathrm{B}} \to \mathrm{D^{**}}\ell\nu)$	$(3.04 \pm 0.44)\%$ [43]	± 0.16
$\mathrm{Br}(\mathrm{b} \to \mathrm{c} \to \ell)$	$(8.4\ ^{+0.42}_{-0.39})\%$ [30]	∓ 0.02
$\mathrm{Br}(\Lambda_\mathrm{b} \to \Lambda_\mathrm{c}\mathrm{X}\ell\nu)$	$(7.9 \pm 1.9)\%$ [14]	∓ 0.06
Total		± 0.19

models as prescribed by the LEP Electroweak Working Group [35].

The lepton spectrum from the b $\to$ c $\to \ell$ decay in the ACCMM model is different from the lepton spectrum in the ISGW model. The systematic error due to the shape of the b $\to$ c $\to \ell$ lepton spectrum is calculated and is found to be negligible. The lepton spectrum from the c $\to \ell$ decay is varied from the ACCMM model to the ISGW model, where the c quark is a primary quark from Z decay. The systematic error is calculated and found to be negligible.

Monte Carlo statistics: The systematic uncertainty due to the limited Monte Carlo statistics is $\pm 0.22 \times 10^{-3}$.

***b* and *c* hadron semileptonic decay branching fractions:** The systematic error is estimated from the uncertainties of the branching fractions of B $\to$ D$\ell\nu$, B $\to$ D$^*\ell\nu$, B $\to$ D$^{**}\ell\nu$ and $\Lambda_\mathrm{b} \to \Lambda_\mathrm{c}\mathrm{X}\ell\nu$. There is a 6.8% background contribution from the b $\to$ c $\to \ell$ decays and a 0.6% background contribution from the c $\to \ell$ decays. The systematic error is also estimated from the uncertainties of the branching fractions of the b $\to$ c $\to \ell$ decays. A summary of these systematic errors from the uncertainties of b hadron and c hadron semileptonic decay branching ratios is shown in Table 2. The $\mathrm{Br}(\bar{\mathrm{B}} \to \mathrm{D^{**}}\ell\nu)$ in Table 2 is obtained by averaging the $\mathrm{Br}(\bar{\mathrm{B}} \to \mathrm{D^{**}}\ell\nu)$ from ARGUS [40], ALEPH [41], DELPHI [42] and the total B semileptonic decay branching fraction subtracting the contribution from B to D and D* semileptonic decay, described by the LEP, CDF and SLD Heavy Flavour Working Group [43]. For the decay of $\bar{\mathrm{B}} \to \mathrm{D^{**}}\ell\nu$, in which D** refers to $\mathrm{D_1}$, $\mathrm{D_2^*}$, $\mathrm{D_2}$ and $\mathrm{D_1^*}$, the branching ratio for each specific D** final state is not well measured. For this analysis, the narrow final states of D** in $\bar{\mathrm{B}} \to \mathrm{D^{**}}\ell\nu$ are replaced by the broad states and then vice-versa to check the sensitivity of the $\mathrm{Br}(b \to \mathrm{X_u}\ell\nu)$ to the relative ratio of the narrow and broad states of D** in $\bar{\mathrm{B}} \to \mathrm{D^{**}}\ell\nu$. The effect on the $\mathrm{Br}(b \to \mathrm{X_u}\ell\nu)$ is found to be negligible.

Monte Carlo modeling errors: The systematic error for the Monte Carlo modeling errors is estimated by reweighting each input variable distribution in the Monte Carlo simulation to agree with the corresponding data distributions. A branching fraction of 1.63×10^{-3} for the $b \to \mathrm{X_u}\ell\nu$ transition is incorporated in the Monte Carlo simulation as shown in Fig. 4. This gives a conservative estimation of the systematic uncertainty due to the modeling of the input variables.

Table 3. $Br(b \to X_u \ell\nu)$ results from ALEPH, DELPHI, L3 and this analysis

Experiment	$Br(b \to X_u \ell\nu)$ (10^{-3})	Ref
ALEPH	1.73 ± 0.56 (stat+det) ± 0.51 (b $\to$ c) ± 0.21 (b $\to$ u)	[4]
DELPHI	1.57 ± 0.46 (stat+det) ± 0.36 (b $\to$ c) ± 0.29 (b $\to$ u)	[5]
L3	3.3 ± 1.3 (stat+det) ± 1.4 (b $\to$ c) ± 0.5 (b $\to$ u)	[6]
OPAL (This analysis)	1.63 ± 0.57 (stat+det) $^{+0.44}_{-0.52}$ (b $\to$ c) ± 0.25 (b $\to$ u)	

***b* → $X_u \ell\nu$ modeling error from the hybrid model:** The boundary between the inclusive and exclusive regions in the hybrid model is varied from 1.5 GeV/c^2 to 0.9 GeV/c^2. This conservatively estimates the systematic error arising from the placement of the boundary between the inclusive and exclusive models. This produces a uncertainty of $\pm 0.19 \times 10^{-3}$ for $Br(b \to X_u \ell\nu)$.

***b* → $X_u \ell\nu$ inclusive model:** The ACCMM model is the base inclusive model. The QCD universal function model and the parton model are used to estimate the systematic errors in the inclusive part of the $b \to X_u \ell\nu$ hybrid model. This gives a change of -0.14 $\times$ 10^{-3} for the QCD universal function model and +0.02 $\times$ 10^{-3} for the parton model for the branching ratio of $b \to X_u \ell\nu$. The largest variation of $Br(b \to X_u \ell\nu)$ from these models is taken as the systematic uncertainty of $Br(b \to X_u \ell\nu)$ from the inclusive model.

***b* → $X_u \ell\nu$ exclusive model:** The ISGW2 model is the base exclusive model. The model implemented in the OPAL tune of JETSET [11] Monte Carlo simulation, which has the u quark and the spectator quark forming one single hadron in the final state, is used to estimate the systematic error in the exclusive part of the $b \to X_u \ell\nu$ hybrid model.

Tracking resolution: The systematic error due to the uncertainties of the detector resolution is estimated by applying a $\pm 10\%$ variation to the r-ϕ track parameters and an independent $\pm 10\%$ variation to the analogous parameters in the r-z plane to the Monte Carlo simulated events [28].

***c* hadron decay multiplicity:** The systematic error of the $Br(b \to X_u \ell\nu)$ associated with the c hadron decay charge multiplicity is estimated using the average charged track multiplicity of D^+, D^0, D_s^+ decays as measured by MARK III [44]. The systematic uncertainty of the $Br(b \to X_u \ell\nu)$ is $\pm 0.07 \times 10^{-3}$ from the uncertainty of c hadron decay multiplicity.

Λ_b production rate: The PDG [14] gives the production fraction of B^+, B^0, B_s^0 and Λ_b in Z decay as (38.9 $\pm$ 1.3)%, (38.9 $\pm$ 1.3)%, (10.7 $\pm$ 1.4)% and (11.6 $\pm$ 2.0)% respectively. The neural network output variable distributions among B^+, B^0 and B_s^0 are similar and the systematic effects caused by the uncertainties of the production fraction of B^+, B^0 and B_s^0 are negligible. Due to the difference of the neural network output variable distributions between Λ_b and B mesons, the fraction of Λ_b is varied by one standard deviation to determine the corresponding systematic error.

Λ_b polarization: The lepton momentum spectrum from Λ_b semileptonic decays depends on the degree of Λ_b polarization. The systematic uncertainties are estimated by using the Λ_b polarization range $\langle P_L^{\Lambda_b} \rangle = -0.56\ ^{+0.22}_{-0.16}$ [26].

Lepton identification efficiency: The number of selected events in the signal and background depends on the electron identification efficiency and the muon identification efficiency. The electron identification efficiency has been studied using control samples of electrons from $e^+e^- \to e^+e^-$ events and photon conversions, and is modeled to a precision of 4% [28]. The muon identification efficiency has been studied by using the muon pairs produced in two-photon collisions and $Z \to \mu^+\mu^-$ events, giving an uncertainty of 2% [30].

Lepton fake rate: Fake electrons in the electron sample are primarily from charged hadrons (mainly charged pions) misidentified as electrons and from untagged photon conversions. The uncertainty associated with electron misidentification is $\pm 21\%$ [28]. The muon fake rate is studied from $K_s^0 \to \pi^+\pi^-$ and $\tau \to 3\pi$ decay. The uncertainty of the fake muon rate is estimated to be $\pm 8\%$.

***b* → $X\tau\bar{\nu}_\tau$ branching ratio:** One important composition in the "other" background in Fig. 5b results from a b quark semileptonic decay to a τ lepton, with the τ lepton subsequently decaying to an electron or a muon. The branching ratio of $b \to X\tau\bar{\nu}_\tau$ is $(2.6 \pm 0.4)\%$ [14]. The systematic error is estimated using the uncertainties of the $b \to X\tau\bar{\nu}_\tau$ branching ratio.

Uncertainty of the *b* lifetime The average b hadron lifetime is measured to be (1.564 ± 0.014) ps [14]. The uncertainty in b lifetime results in a negligible uncertainty in $Br(b \to X_u \ell\nu)$.

Uncertainty of R_b: The fraction of $Z \to b\bar{b}$ events in hadronic Z decays, R_b, is measured to be 0.21644 ± 0.00075 [14]. The uncertainty in R_b results in a negligible uncertainty in the background composition.

8 Conclusion

The branching fraction of the inclusive $b \to X_u \ell\nu$ decay is measured to be:

$$Br(b \to X_u \ell\nu) = (1.63 \pm 0.53\ (\text{stat})\ ^{+0.55}_{-0.62}\ (\text{sys})) \times 10^{-3}.$$

The first error 0.53 is the statistical error from the data only. The errors associated with the limited statistics of the Monte Carlo sample are included in the systematic

error. This result is consistent with similar measurements from ALEPH, DELPHI and L3, the other three LEP experiments, shown in Table 3. In Table 3, the first error in $Br(b \to X_u \ell\nu)$ combines the statistical error from the data and limited Monte Carlo statistics as well as the uncorrelated systematic uncertainties due to experimental systematic errors, such as detector resolution and lepton identification efficiency. The second error contains the systematic uncertainties from the $b \to X_c \ell\nu$ Monte Carlo simulation models. The third error contains the systematic uncertainties from the $b \to X_u \ell\nu$ models. The second and third errors are correlated between the various experiments.

$|V_{ub}|$ can be obtained from $Br(b \to X_u \ell\nu)$ [45,46] with inputs slightly revised as described by the LEP Heavy Flavour Working Group [43] in the context of the Heavy Quark Expansion [7]:

$$|V_{ub}| = 0.00445 \times \left(\frac{Br(b \to X_u \ell\nu)}{0.002} \frac{1.55\text{ps}}{\tau_b} \right)^{\frac{1}{2}} \times (1 \pm 0.010_{\text{pert}} \pm 0.030_{1/m_b^3} \pm 0.035_{m_b}), \quad (3)$$

where the average b hadron lifetime τ_b is equal to (1.564 $\pm$ 0.014) ps [14]. Thus, $|V_{ub}|$ obtained from this analysis is:

$$|V_{ub}| = (4.00 \pm 0.65\ (\text{stat})\ ^{+0.67}_{-0.76}\ (\text{sys}) \pm 0.19\ (\text{HQE})) \times 10^{-3},$$

where the systematic error includes the b to u and b to c semileptonic decay modeling error, and the HQE error is purely the theoretical error from the Heavy Quark Expansion. This result is consistent with the $|V_{ub}|$ value from the CLEO exclusive measurement of $(3.3 \pm 0.8\ (\text{total})) \times 10^{-3}$ [47].

Acknowledgements. We particularly wish to thank the SL Division for the efficient operation of the LEP accelerator at all energies and for their continuing close cooperation with our experimental group. We thank our colleagues from CEA, DAPNIA/SPP, CE-Saclay for their efforts over the years on the time-of-flight and trigger systems which we continue to use. In addition to the support staff at our own institutions we are pleased to acknowledge the Department of Energy, USA, National Science Foundation, USA, Particle Physics and Astronomy Research Council, UK, Natural Sciences and Engineering Research Council, Canada, Israel Science Foundation, administered by the Israel Academy of Science and Humanities, Minerva Gesellschaft, Benoziyo Center for High Energy Physics, Japanese Ministry of Education, Science and Culture (the Monbusho) and a grant under the Monbusho International Science Research Program, Japanese Society for the Promotion of Science (JSPS), German Israeli Bi-national Science Foundation (Fig), Bundesministerium für Bildung und Forschung, Germany, National Research Council of Canada, Research Corporation, USA, Hungarian Foundation for Scientific Research, OTKA T-029328, T023793 and OTKA F-023259.

References

1. N. Cabibbo, Phys. Rev. Lett. **10**, 531 (1963); M. Kobayashi, K. Maskawa, Prog. Theor. Phys. **49**, 652 (1973)
2. ARGUS Collaboration, H. Albrecht et al., Phys. Lett. **B234**, 409 (1990)
3. CLEO Collaboration, R. Fulton et al., Phys. Rev. Lett. **64**, 16 (1990); CLEO Collaboration, J. Bartelt, Phys. Rev. Lett. **71**, 4111 (1993)
4. ALEPH Collaboration, R. Barate et al., Eur. Phys. J. **C6**, 555 (1999)
5. DELPHI Collaboration, P. Abreu et al., Phys. Lett. **B478**, 14 (2000)
6. L3 Collaboration, M. Acciarri et al., Phys. Lett. **B436**, 174 (1998)
7. A.H. Hoang, Z. Ligeti, A.V. Manohar, Phys. Rev. **D59**, 074017 (1999); A.H. Hoang, Z. Ligeti, A.V. Manohar, Phys. Rev. Lett. **82**, 277 (1999)
8. CLEO Collaboration, B.H. Behrens et al., Phys. Rev. **D61**, 052001 (2000)
9. OPAL Collaboration, K. Ahmet et al., Nucl. Instrum. Methods **A305**, 275 (1991); P.P. Allport et al., Nucl. Instrum. Methods **A324**, 34 (1993); P.P. Allport et al., Nucl. Instrum. Methods **A346**, 476 (1994)
10. T. Sjöstrand, Comp. Phys. Comm. **82**, 74 (1994)
11. OPAL Collaboration, G. Alexander et al., Z. Phys. **C69**, 543 (1996)
12. C. Ramirez, J.F. Donoghue, G. Burdman, Phys. Rev. **D41**, 1496 (1990)
13. J. Allison et al., Nucl. Instrum. Meth. **A317**, 47 (1992)
14. D.E. Groom et al., Eur. Phys. J. **C15**, 1 (2000)
15. B. Grinstein, M.B. Wise, N. Isgur, Phys. Rev. Lett. **56**, 298 (1986)
16. N. Isgur, D. Scora, B. Grinstein, M. B. Wise, Phys. Rev. **D39**, 799 (1989)
17. M. Wirbel, B. Stech, M. Bauer, Z. Phys. **C29**, 637 (1985); J.G. Körner, G.A. Schuler, Z. Phys. **C38**, 511 (1988)
18. D. Scora, N. Isgur, Phys. Rev. **D52**, 2783 (1995)
19. G. Altarelli, N. Cabibbo, G. Corbò, L. Maiani, G. Martinelli, Nucl. Phys. **B208**, 365 (1982)
20. T. Mannel, M. Neubert, Phys. Rev. **D50**, 2037 (1994)
21. M. Neubert, Phys. Rev. **D49**, 4623 (1994)
22. R.D. Dikeman, M. Shifman, N.G. Uraltsev, Int. J. Mod. Phys. **A11**, 571 (1996)
23. A. Bareiss, E.A. Paschos, Nucl. Phys. **B327**, 353 (1989)
24. M. Jezabek, J.H. Kühn, Nucl. Phys. **B314**, 1 (1989)
25. C. Peterson, D. Schlatter, I. Schmitt, P. M. Zerwas, Phys. Rev. **D27**, 105 (1983)
26. OPAL Collaboration, G. Abbiendi et al., Phys. Lett. **B444**, 539 (1998)
27. OPAL Collaboration, R. Akers et al., Z. Phys. **C66**, 555 (1995)
28. OPAL Collaboration, G. Abbiendi et al., Eur. Phys. J. **C8**, 217 (1999)
29. OPAL Collaboration, R. Akers et al., Z. Phys. **C63**, 197 (1994)
30. OPAL Collaboration, G. Abbiendi et al., Eur. Phys. J. **C13**, 225 (2000)
31. C. Peterson, T. Rognvaldsson, L. Lonnblad, Comp. Phys. Comm. **81**, 185 (1994)
32. G. Bahan, R. Barlow, Comp. Phys. Comm. **74**, 199 (1993)
33. OPAL Collaboration, R. Akers et al., Z. Phys. **C66**, 19 (1995)
34. OPAL Collaboration, K. Ackerstaff et al., Z. Phys. **C74**, 413 (1997)
35. The LEP collaborations, ALEPH, DELPHI, L3 and OPAL, Nucl. Instrum. Methods **A378**, 101 (1996)

36. CLEO Collaboration, R. Fulton et al., Phys. Rev. **D43**, 651 (1991)
37. SLD collaboration, K. Abe et al., Phys. Rev. Lett. **84**, 4300 (2000)
38. P.D.B. Collins, T.P. Spiller, J. Phys. **G11**, 1289 (1985)
39. V.G. Kartvelishvili, A.K. Likhoded, V.A. Petrov, Phys. Lett. **B78**, 615 (1978)
40. ARGUS Collaboration, H. Albrecht et al., Z. Phys. **C57**, 533 (1993)
41. ALEPH Collaboration, D. Buskulic et al., Z. Phys. **C73**, 601 (1997)
42. DELPHI Collaboration, P. Abreu et al., Phys. Lett. **B475**, 407 (2000)
43. ALEPH Collaboration, CDF Collaboration, DELPHI Collaboration, L3 Collaboration, OPAL Collaboration and SLD Collaborations, D. Abbaneo et al., "Combined results on B hadron production rates, lifetimes, oscillations and semileptonic decays", SLAC-PUB-8492, CERN-EP-2000-096 (2000)
44. MARK III Collaboration, D. Coffman et al., Phys. Lett. **B263**, 135 (1991)
45. I. Bigi, R.D. Dikeman, N. Uraltsev, Eur. Phys. J. **C4**, 453 (1998)
46. N. Uraltsev, Int. J. Mod. Phys. **A14**, 4641 (1999)
47. CLEO Collaboration, J.P. Alexander et al., Phys. Rev. Lett. **77**, 5000 (1996)